Resonant multiple-phonon absorption causes efficient anti-Stokes photoluminescence in CsPbBr₃ nanocrystals

Zhuoming Zhang^{1†}, Sushrut Ghonge^{2†}, Yang Ding¹, Shubin Zhang², Mona Berciu^{3,4*}, Richard D. Schaller^{5,6}, Boldizsár Jankó^{2*}, Masaru Kuno^{1,2*}

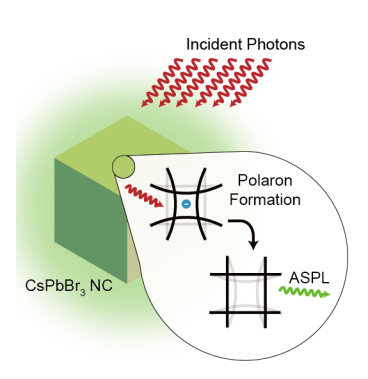
- Department of Chemistry and Biochemistry, University of Notre Dame, 251 Nieuwland Science Hall, Notre Dame, IN 46556, United States
- Department of Physics and Astronomy, University of Notre Dame, 225 Nieuwland Science
 Hall, Notre Dame, IN 46556, United States
- 3. Department of Physics and Astronomy, University of British Columbia, Vancouver Campus 325-6224, Agricultural Road, Vancouver BC V6T 1Z1, Canada
 - 4. Stewart Blusson Quantum Matter Institute, University of British Columbia, Vancouver,
 British Columbia, V6T 1Z4 Canada
 - 5. Department of Chemistry, Northwestern University, Evanston, IL 60208
- 6. Center for Nanoscale Materials, Argonne National Laboratory, Lemont, IL 60439, United States

† contributed equally

E-mail: berciu@phas.ubc.ca, bjanko@nd.edu and mkuno@nd.edu

ABSTRACT. Lead-halide perovskite nanocrystals such as CsPbBr₃, exhibit efficient photoluminescence (PL) up-conversion, also referred to as anti-Stokes photoluminescence (ASPL). This is a phenomenon where irradiating nanocrystals up to 100 meV below gap results in higher energy band edge emission. Most surprising is that ASPL efficiencies approach unity and involve single photon interactions with multiple phonons. This is unexpected given the statistically disfavored nature of multiple-phonon absorption. Here, we report and rationalize near-unity anti-Stokes photoluminescence efficiencies in CsPbBr₃ nanocrystals and attribute it to resonant multiple-phonon absorption by polarons. The theory explains paradoxically large efficiencies for intrinsically disfavored, multiple-phonon-assisted ASPL in nanocrystals. Moreover, the developed microscopic mechanism has immediate and important implications for applications of ASPL towards condensed phase optical refrigeration.

KEYWORDS: photoluminescence, lead halide perovskite, nanocrystal, polaron, optical refrigeration, anti-Stokes photoluminescence, up-conversion photoluminescence



TOC graphic

Unlike most other materials, lead halide perovskites, a new class of materials, interact with light differently in two important ways. First, they readily exhibit near-unity photoluminescence (PL) quantum yields (QYs), where QY is defined as the ratio of emitted photons to absorbed photons. A QY of less than unity indicates non-radiative relaxation processes in the material that lead to heating. Second, they show efficient anti-Stokes photoluminescence (ASPL), where emitted photons have greater energy than those absorbed. The ASPL energy difference, ΔE , represents heat extracted from the material. Making lead halide perovskite nanocrystals special are near-unity ASPL efficiencies, η_{ASPL} , defined as the fraction of absorbed photons re-emitted at higher energy. A material that simultaneously possesses near-unity QYs and large η_{ASPL} -values can cool when irradiated with light.

Condensed phase optical refrigeration can, in principle, be achieved via ASPL with important practical applications in vibration-free cryocoolers^{1,2,3} and radiation-balanced lasers^{4,5}. While optical refrigeration of solids was first conceived by Pringsheim⁶ in 1929, the phenomenon has been demonstrated only recently⁷ with rare earth-doped glasses/crystals cooled from room temperature to ~91 K. ⁸ Going to lower temperatures requires optically refrigerating semiconductors.^{9,10}

To this end, cesium lead tribromide (CsPbBr₃) perovskite nanocrystals (NCs) are intriguing materials for demonstrating semiconductor optical refrigeration. ¹¹ This stems from their soft lattice and strong electron-phonon coupling, which readily leads to polaron formation. ^{12,13,14,15} More importantly, CsPbBr₃ NCs exhibit near-unity, ASPL efficiencies, with previously reported η_{ASPL} -values of η_{ASPL} -75% (η_{ASPL} -32%) for a ΔE =24 meV (102 meV) detuning into the gap. ¹⁶ Absorption of multiple phonons by photoexcited carriers is hypothesized to be responsible for large ASPL efficiencies. ^{11,17} However, given longitudinal optical (LO) phonon energies, ranging from 4-44 meV [See Supporting Information (SI), Table S1], ^{18,19,20,21,22,23,24} 1-25 LO phonons must be involved in the up-conversion process.

Multiple-phonon processes are responsible for intra- and inter-band relaxation in semiconductors. ^{25,26,27} They dictate whether phenomena such as hot carrier extraction ^{28,29} and phonon bottlenecks ^{30,31} are observed. Whereas multiple-phonon emission is efficient, the opposite is not. Multiple-phonon absorption requires fast multiple-phonon interactions with photogenerated carriers. Absorption rates increase with electron-phonon coupling energies and decrease exponentially with the number of phonons involved. This makes multiple-phonon absorption processes exceedingly rare.

Despite this, multiple-phonon absorption can be experimentally observed via single-photon/multiple-phonon anti-Stokes photoluminescence (ASPL).^{16, 32, 33} The process entails photoexciting semiconductors below their optical gap whereupon interacting with lattice phonons raises the energy of incident excitations to the band edge. Subsequent band gap photoluminescence confirms multiple-phonon-assisted up-conversion. Despite active efforts in the area^{17,34,35,36,37,38,39}, an open question remains whether near-unity ASPL efficiencies are possible given intrinsically disfavored multiple-phonon absorption rates.

Results/Discussion

We now posit the mechanism for efficient ASPL and the origin of near-unity η_{ASPL} -values in CsPbBr₃ NCs. Visible photothermal absorption (PA) as well as Stokes-photoluminescence (PL) and ASPL spectroscopies are used to map η_{ASPL} across a wide range of temperatures and below gap detuning energies. Observed η_{ASPL} -values are near-unity as well as non-Arrhenius. They are rationalized using a resonant multiple-phonon absorption model, developed below.

Quaternary ammonium passivated CsPbBr₃ NCs were synthesized via literature procedures. 40,41 Benzoyl bromide was introduced to pre-made Cs-Pb-oleate to trigger NC

growth. Particles were subsequently passivated with didodecyl dimethyl ammonium bromide (DDDMABr), washed with ethyl acetate, and redispersed in toluene. A CsPbBr₃ NC/polystyrene matrix (75000 MW, 5% w/w in toluene) was prepared and drop cast onto sapphire for optical measurements. Details of the sample preparation can be found in the Materials and Methods section.

For representative CsPbBr₃ NCs (**Figure 1**), an average edge length is l=6.8±0.7 nm (N=957, **Figure 1a, inset**, and **Figure S1**). A corresponding, room temperature linear absorption spectrum reveals a first excitonic peak at 500 nm and band edge PL at 506 nm ($\lambda_{\rm exc}$ =450 nm, solid green line, 30 meV Stokes-shift^{42,43}). Accompanying ASPL (open red circles), obtained by exciting below the peak PL energy ($\lambda_{\rm exc}$ =535 nm, ΔE =132 meV), reveals little to no difference in observed spectral characteristics. This confirms up-conversion to the same emitting state.

Excitation intensity (I_{exc})-dependent PL measurements show linear behavior over two orders of magnitude in I_{exc} . This establishes that observed ASPL involves single-photon/multiple-phonon up-conversion (**Figure 1b**) and agrees with past observations by us¹⁶ and others⁴⁴. Additional measurements show ASPL for energetic detuning up to ΔE =153 meV (**inset**, **Figure 1b**). Beyond this, ASPL arises from two-photon up-conversion, as observed via quadratic I_{ASPL} versus I_{exc} dependencies. See **Figure S2** for more information.

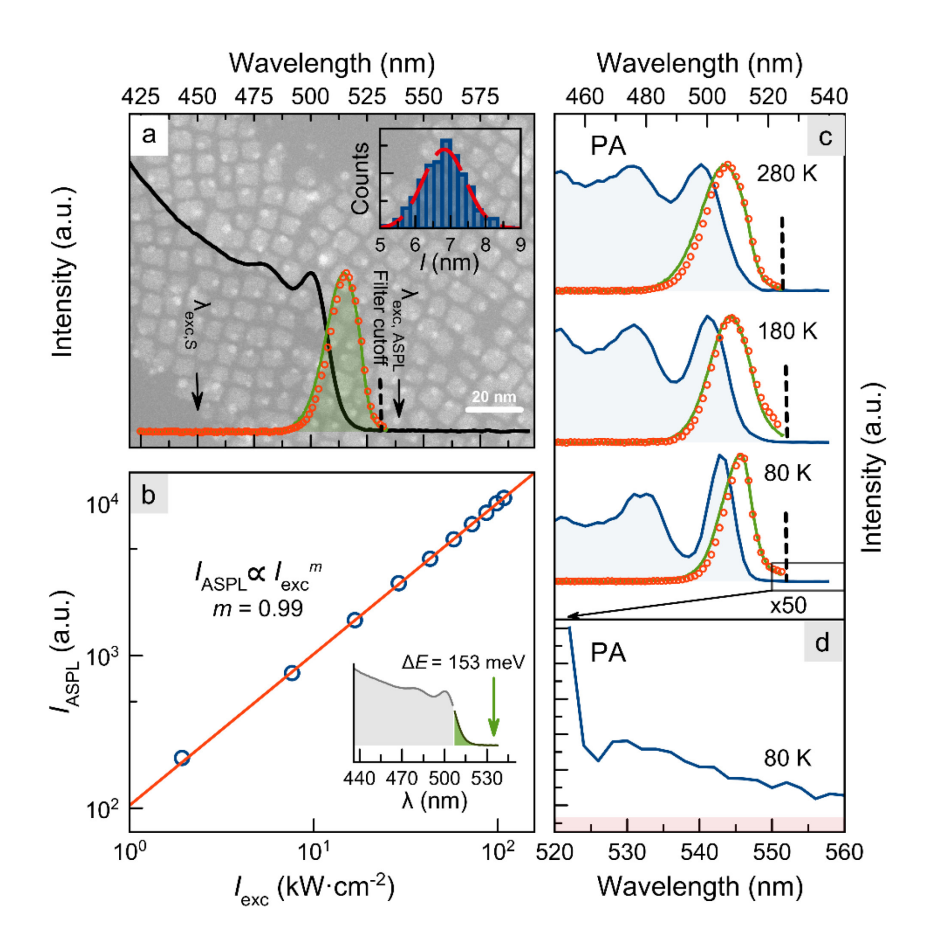


Figure 1. Experimental CsPbBr₃ NC ASPL data. (a) CsPbBr₃ NC (l=6.8±0.7 nm) ensemble linear absorption (black), Stokes PL (green, $\lambda_{\rm exc}$ =450 nm), and ASPL (open red circles, $\lambda_{\rm exc}$ =535 nm) spectra. Representative STEM image with associated size distribution histogram (inset). (b) $I_{\rm exc}$ -dependent $I_{\rm ASPL}$ ($\lambda_{\rm exc}$ =535 nm, ΔE = 153 meV). Solid red line, linear fit. Inset: Excitation range for single-photon/multiple-phonon up-conversion (green fill). (c) PA (solid blue line/fill), PL (solid green line), and ASPL (open red circles) spectra at 280 K, 180 K and 80 K. Vertical dash lines, filter cutoff. (d) Anti-Stokes PA spectrum at 80 K, baseline shaded red.

Detailed η_{ASPL} dependencies with temperature (T) and ΔE are investigated to establish mechanistic insight into underlying multiple-phonon interactions. Whereas η_{ASPL} has previously

been estimated using experimental absorptance and I_{exc} -values that match PL and ASPL intensities 16 , a different approach is used here to more broadly access a wide range of T and ΔE . PL and ASPL spectral pairs are acquired between T=80 and 280 K for different Stokes (anti-Stokes) detuned energies ΔE_{S} =170-480 meV (ΔE =20-153 meV) above (below) the emitting state. Photothermal absorption (PA) 45,46 measurements are simultaneously conducted to estimate the amount of absorbed above/below gap light. The importance of PA measurements rests with its ability to discriminate against scattering contributions to NC extinction as well as its sensitive nature, which enables low cross section states to be observed. Details about employed PL, ASPL, and PA measurements as well as an experimental schematic can be found in the **Methods** and in **Scheme S1**.

Acquired PL, ASPL, and PA data at three temperatures (280 K, 180 K, and 80 K) are summarized in **Figure 1c**. For clarity PL and ASPL spectra have been normalized to each other. **Figure S3** summarizes all 11 temperatures studied. Acquired PA spectra reproduce band edge excitonic features, first seen in **Figure 1a**. With decreasing temperature, PL, ASPL and PA spectra all line-narrow and redshift slightly. The **SI** summarizes observed PA and PL Varshni relationships, spectral linewidths, and empirical T-dependent peak absorption/peak emission energy differences. ⁴⁷ Analogous PL and ASPL behavior are observed for all ΔE_S and ΔE employed (**Table S2** and **Figure S4**).

Figure 2a now shows relevant absorption and emission processes used to model experimental PL (I_S) and ASPL (I_{AS}) intensities as well as above/below gap PA. Explicit model expressions for I_S and I_{ASPL} are

$$I_{\rm S} \propto {\rm QY}(I_{\rm exc.S}A_{\rm S})$$
 (1)

and

$$I_{\rm AS} \propto \eta_{\rm ASPL} \, {\rm QY} \big(I_{\rm exc,AS} A_{\rm AS} \big)$$
 (2)

where QY is the specimen's emission quantum yield and $I_{\text{exc,S}}$ ($I_{\text{exc,AS}}$) is the Stokes (anti-Stokes) excitation intensity with A_{S} (A_{AS}) associated absorptances. Corresponding Stokes and anti-Stokes PA expressions are

$$PA_S \propto (I_{exc,S}A_S)[\Delta E_S + (1 - QY) \cdot E_g]$$
 (3)

and

$$PA_{AS} \propto (I_{exc,AS}A_{AS})[(1 - \eta_{ASPL}QY)E_g - \Delta E].$$
 (4)

The latter PA equations are energy conserving and reflect heat generation due to non-radiative relaxation that follows absorption. More details can be found in the SI.

Equations 1-4 enable η_{ASPL} to be extracted as functions of T and ΔE via a function, R, defined in terms of the ratio of I_{ASPL}/PA_{AS} to I_{S}/PA_{S} , *i.e.*,

$$R(\Delta E_S, \Delta E, \eta_{\text{ASPL}}, \text{QY}) = \frac{\eta_{\text{ASPL}}[E_g \cdot (1 - \text{QY}) + \Delta E_s]}{E_g \cdot (1 - \eta_{\text{ASPL}} \cdot \text{QY}) - \Delta E}.$$
 (5)

R depends linearly with $\Delta E_{\rm S}$ for fixed ΔE , allowing $\eta_{\rm ASPL}$ and QY to be extracted via global fits of obtained R for fixed ΔE at different T. Details of the procedure can be found in the **Methods** and in the **SI**.

Figure 2b shows experimental R for ΔE =23 meV (red), ΔE =33 meV (blue), and ΔE =46 meV (green). Figure S5 (Table S3) summarizes R (η_{ASPL}) for all ΔE . Associated linear fits yield QY=0.84 and η_{ASPL} -values that decrease non-linearly from η_{ASPL} = 0.75 (ΔE =23 meV) to η_{ASPL} =0.32 (ΔE =102 meV). Figure 2c summarizes this behavior. Note that the fit-extracted QY is in good agreement with specimen QY values, obtained using two independent approaches. The first involves power-dependent photoluminescence measurements of NC films to yield QY=0.84 (Figure S7a). 48,49 The second uses an integrating sphere on a colloidal NC suspension to yield QY=0.87 (Figure S7b). Details of these measurements can be found in the SI.

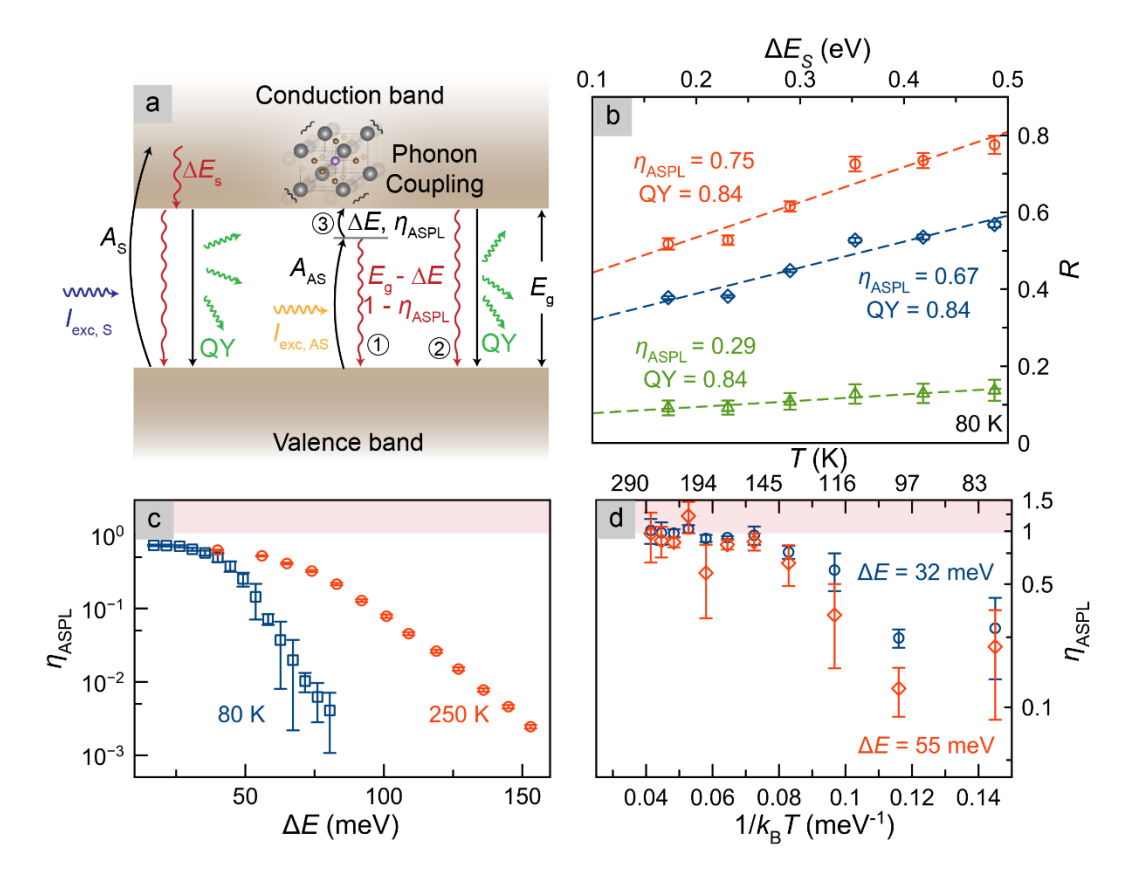


Figure 2. CsPbBr₃ NC η_{ASPL} temperature and excitation energy de-tuning dependencies. (a) Schematic of relevant PL, ASPL, and PA processes. (b) R as a function of ΔE_S for ΔE =23 meV (red circle), ΔE =33 meV (blue diamond), and ΔE =46 meV (green triangle). (c) Extracted η_{ASPL} ΔE -dependency at 80 K (open blue squares) and 250 K (open red circles), η_{ASPL} =1 shadowed red. (d) Extracted η_{ASPL} T-dependency for ΔE =32 meV (open blue circles) and 55 meV (open red diamonds), η_{ASPL} =1 shadowed red.

Figure 2d shows η_{ASPL} T-dependencies with data plotted versus $1/k_{\text{B}}T$. Figure S5 (Table S4) summarizes R (η_{ASPL}) for T=80-280 K for ΔE =32 meV and ΔE =55 meV. With increasing T, η_{ASPL} approaches unity. Log[η_{ASPL}] does not, however, increase linearly as expected of Arrhenius behavior. This is noteworthy given previous reports suggesting $\eta_{\text{ASPL}} \propto e^{-\frac{\Delta E}{k_{B}T}}$ for both CdS nanobelts⁵⁰ and CsPbBr₃ NCs.⁴⁴ Figures 2b and 2c point to non-Arrhenius η_{ASPL} .

Up-conversion is now modeled as an interacting two-level system, consisting of valence bandedge $|v\rangle$ and conduction band-edge $|c\rangle$ states, coupled to a phonon mode with energy ω_p . Electron-phonon coupling is described using $g|c\rangle\langle c|(b^{\dagger}+b)$, where b^{\dagger} and b are phonon creation and annihilation operators, and g is the electron-phonon coupling constant (**Table S1**). The effective Hamiltonian, H, acting on the electron Hilbert space and phonon Fock space, is given by

$$H = E_{\nu}|\nu\rangle\langle\nu| + E_{c}|c\rangle\langle c| + \omega_{\nu}b^{\dagger}b + g|c\rangle\langle c|(b^{\dagger} + b).$$
 (6)

Eigenstates consist of polarons (conduction band states dressed with *n* phonons) and similarly dressed valence band states,

$$|c_n\rangle = |c\rangle \otimes \frac{(B^{\dagger})^n}{\sqrt{n!}} |\tilde{0}\rangle \quad \text{and} \quad |v_n\rangle = |v\rangle \otimes \frac{(b^{\dagger})^n}{\sqrt{n!}} |0\rangle.$$
 (7)

 B^{\dagger} is the dressed-phonon creation operator, $B^{\dagger}=b^{\dagger}+g/\omega_{p}$, with a coherent vacuum state,

 $|\tilde{0}\rangle=e^{-\frac{g^2}{2\omega_p^2}-\frac{g}{\omega_p}b^\dagger}|0\rangle$. Corresponding conduction (valence) band energies are $E(c_n)=E_c+n\omega_p-g^2/\omega_p$ $[E(v_n)=E_v+n\omega_p]$ with an associated polaron energy of $E_c-\frac{g^2}{\omega_p}$.

At thermal equilibrium, the probability of occupying a *n*-phonon state is $e^{(-n\omega_p/k_BT)}/Z$, where *Z* is the partition function. Using the Kramers-Heisenberg equation for resonant phonon absorption⁵¹, the *N*-phonon absorption rate is

$$w_N = \left| \sum_{n=0}^{\infty} \frac{\langle N | \tilde{n} \rangle \langle \tilde{n} | 0 \rangle}{n \omega_p + i \zeta} \right|^2 \delta \left(N \omega_p - \Delta E \right)$$
 (8)

where ζ is the conduction band recombination rate and $|\tilde{n}\rangle = [(B^{\dagger})^n/\sqrt{n!}]|\tilde{0}\rangle$. In turn, the upconversion rate, $w_{\rm uc}$, is the weighted sum of phonon absorption rates with all possible initial states, i.e., $w_{\rm uc} = \sum_N (e^{-N\omega_p/k_BT}/Z)w_N$. Keeping only the resonant term (n=0) and substituting $N = \frac{\Delta E}{\omega_p}$ from the Dirac delta function, yields

$$w_{\rm uc} \propto \frac{e^{-\frac{\Delta E}{k_B T}}}{\sqrt{\Delta E}} \exp\left[\frac{\Delta E}{\omega_p} \left(1 - \log\frac{\Delta E \omega_p}{g^2}\right)\right],$$
 (9)

which is non-Arrhenius, thus rationalizing observed non-Arrhenius behavior in **Figures 2c** and **2d**.

Figure 3 compares experimental η_{ASPL} with Equation 9 where $\eta_{\text{ASPL}}(T, \Delta E) = \frac{w_{\text{uc}}(T, \Delta E)}{w_{\text{r}}}$ with $w_{\text{r}} = w_{\text{uc}} + w_{\text{nr}}$ the total depopulation rate, including nonradiative recombination. Evident is that resonant multiple-phonon absorption by polarons quantitatively accounts for η_{ASPL} ΔE - and T-dependencies. Extracted electron-phonon coupling and phonon energies are: 80 K, g=21.4±0.34 meV, $\omega_p = 5.17 \pm 0.27$ meV; 250 K, g=41.1±0.58 meV, $\omega_p = 23.4 \pm 2.2$ meV. Model-extracted ω_p and g are in good agreement with LO phonon and electron-LO phonon coupling energies previously reported for CsPbBr₃ (**Table S1**).

Ab-initio calculations^{23,24} show phonons with energies 4-7 meV (Cs vibrations in the Cs-Br plane and rotation of PbBr₆ octahedra), 9.5 meV (Cs-Br in-plane motion), and 18-19 meV (Pb-Br stretching mode in the PbBr₂ plane). Observed *T*-dependent differences in ω_p and possibly g may reflect variations to the dominant phonon mode, given changes to the Bose-Einstein distribution at 80 K ($k_BT \approx 7$ meV) and 250 K ($k_BT \approx 22$ meV). Direct identification of involved phonon modes would require observing an isotope effect wherein ω_p scales with the inverse square root of the isotope mass.

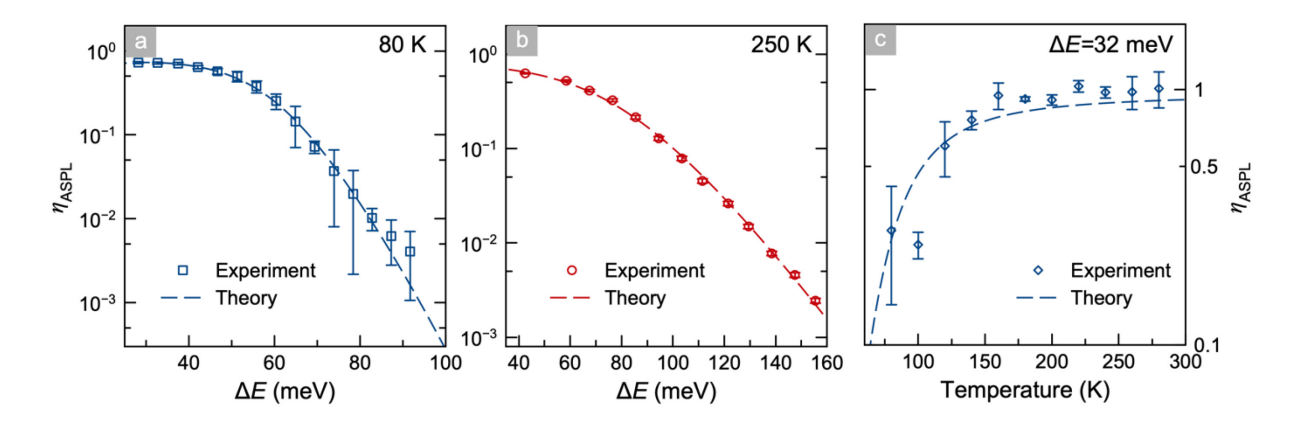


Figure 3. CsPbBr₃ NC η_{ASPL} comparison between experiment and theory. Model (dashed lines) and experimental (symbols) η_{ASPL} ΔE dependency comparison at (a) 80 K and (b) 250 K. (c) Analogous η_{ASPL} T-dependent comparison for fixed ΔE =32 meV.

Although the model does not explicitly predict numerical values for up-conversion rates, given that η_{ASPL} depends on both w_{uc} and w_{nr} , we performed ultrafast transient up-conversion absorption experiments using a 5 kHz amplified Ti:S laser with an 80 fs pulsewidth to estimate w_{uc} . Results from these measurements with NCs excited below gap at varying ΔE (**Figure S8** and **Table S5**) suggest that up-conversion timescales range from 52-220 fs for ΔE =33-100 meV. Given η_{ASPL} in the range η_{ASPL} =0.2-0.8, $1/w_{\text{nr}}$ ranges from 13-880 fs. This points to multiple-phonon absorption becoming competitive with non-radiative relaxation.

Our model implies that the polaron binding energy $\left(\frac{g^2}{\omega_p}\right)$ contributes to the Stokes shift (*i.e.*, the difference in energy between band edge absorption and emission peaks). Originally, a confined hole state model predicted NC Stokes shifts of sizable magnitude.⁴³ More recent DFT calculations, which directly included spin-orbit coupling effects, however, revealed that the confined hole state transition was not dark.⁴² This prompted further efforts to find an explanation

for perovskite NC Stokes shifts. While band edge exciton fine structure from both spin-orbit coupling and the electron-hole exchange interaction does split ground state excitons into dark (singlet) and bright (triplet) states ^{52,53}, observed dark/bright exciton splittings are much too small (<10 meV) to rationalize size-dependent 20-80 meV Stokes shifts seen in CsPbBr₃ NC ensembles.

The polaron model, which involves phonon-dressed states, preserves exciton fine structure and together with its polaron binding energy may ultimately rationalize the overall magnitude of experimental Stokes shifts. Note though that a full theoretical description of a polaron-based Stokes shift has yet to be developed.

Conclusion

In summary, we find that efficient, multiple-phonon-assisted ASPL in CsPbBr₃ NCs is a consequence of resonant phonon absorption by polarons caused by strong electron-phonon coupling. Resonant absorption makes possible counterintuitive, near-unity η_{ASPL} despite sizable sub-gap detuning energies. Moreover, the developed model broadly rationalizes near-ubiquitous, single-photon/multiple-phonon PL up-conversion in semiconductor NCs, identifies resonant multiple-phonon absorption by polarons as the origin of CsPbBr₃ NC up-conversion, points to simultaneous near-unity PL quantum yields and near-unity η_{ASPL} -values being self-consistent, and possibly leads to rational approaches for discovering and engineering materials capable of efficient anti-Stokes photoluminescence.

Methods/Experimental

Chemicals. Lead (II) acetate trihydrate (PbOAc₂•3H₂O, 99.99%), cesium carbonate (Cs₂CO₃, 99%), 1-octadecene (ODE, 90%), didodecyl dimethyl ammonium bromide (DDDMABr, 98%), ethyl acetate (EtOAc, 98.8%), toluene (anhydrous, 99.6%), and polystyrene (PS, 75000 MW) were purchased from Sigma Aldrich. Oleic acid (OA, 99%), benzoyl bromide (BzBr, 97%), and didodecylamine (DDAm, 97%) were purchased from TCI. All chemicals were used as received.

CsPbBr₃ NC synthesis and purification. CsPbBr₃ NCs were synthesized using a modified literature procedure. ⁴⁰ In brief, a Cs-Pb cationic stock solution was prepared by mixing Cs₂CO₃ (760 mg, 2 mmol) and PbOAc₂*3H₂O (160 mg, 0.50 mmol) in a three-neck flask, followed by injection of 10 mL of OA. The mixture was then degassed under a pressure of < 20 mbar on a Schlenk line for three hours at 100 °C to produce Cs-Pb-oleate and remove carbonic and acetic acid byproducts. The resulting product was stored under nitrogen. An accompanying BzBr stock solution was prepared by dissolving 1.0 mL (8.5 mmol) of BzBr in 10 mL of toluene. A surface passivating DDDMABr stock solution was prepared by dissolving 0.231 g (0.5 mmol) of DDDMABr in 20 mL of toluene.

CsPbBr₃ NCs were synthesized in a nitrogen atmosphere glovebox. 750 µL of the Cs-Pb stock solution was mixed with 5 mL of ODE and 221.5 mg (0.63 mmol) of DDAm in a 20 mL scintillation vial. The vial was inserted into an aluminum block, set atop a magnetic stir plate. The Al block's temperature was then raised to values between 70 °C and 110 °C, depending on desired NC size. Once the final growth temperature was reached, the vial was removed whereupon 0.55 mL of the BzBr stock solution was injected to initiate NC growth. An immediate color change from clear to yellow was observed. The reaction was subsequently allowed to cool to room temperature.

After cooling, 2 mL (50 mmol) of a surface passivating DDDMABr stock solution was added to 3 mL aliquots of as-prepared NCs to replace their original oleate ligands. An immediate photoluminescence brightening of ensembles results. 16 mL of EtOAc was subsequently added followed by centrifugation at 4400 rpm to recover a NC precipitate. Recovered NCs were resuspended in neat toluene for subsequent optical measurements. Samples were filtered through 0.22 μm PTFE filters to remove any particulates.

Characterization. Scanning transmission electron microscopy (STEM) images were acquired with a Spectra 300 microscope (Thermo Scientific), operating an accelerating voltage of 300 kV. Samples were prepared by drop-casting dilute NC solutions in toluene onto ultrathin amorphous carbon substrates with copper supports (Ladd). ImageJ was used to estimate NC edge lengths via its FIJI Particle Analysis Procedure. NC edge lengths were then obtained as square roots of obtained areas. NC shapes are implicitly assumed to be cubic.

Optical sample preparation. A polystyrene (PS) stock solution was prepared by dissolving 50 mg of PS in 950 mg toluene (5% w/w PS solution in toluene). The mixture was stirred at 50 °C until clear. For optical measurements, 1 mL aliquots of NC ensembles were mixed with an equivalent volume of the PS stock solution. The resulting mixture was then drop-cast onto 1 mm thick sapphire substrates (Esco Optics).

Visible photothermal absorption spectroscopy. A fiber-based supercontinuum laser (NKT, SuperK extreme), coupled to an acousto optical filter was used as a tunable, visible wavelength excitation source. The supercontinuum intensity was modulated at 4 kHz using a mechanical chopper (Thorlabs, MC2000). Intensity modulated light was then focused onto NC specimens using a 0.4 numerical aperture (NA) long working distance objective (Mitutoyo).

The specimen was mounted to the cold finger of an optical microscope cryostat (Cryo Industries of America). During measurements, specimen temperatures were varied from 80 K to 280 K with a temperature controller (Lakeshore). The cryostat was actively pumped using a turbo pump with its base pressure maintained at 10⁻⁵ torr.

A continuous-wave, red probe laser (785 nm, Coherent OBIS) was simultaneously focused onto the specimen from the opposite (counterpropagating) direction. A 0.45 NA objective (Nikon) was used to focus the probe light. Pump (average) and probe intensities at the sample were 22 kW cm⁻² and 15 MW cm⁻² respectively.

Scattered probe light was collected using the same Nikon objective and was directed onto a photodiode (Thorlabs, PDA36A). The photodiode signal was then fed into a lock-in amplifier (Stanford Research Systems, SR 830), referenced to the mechanical chopper. A typical lock-in integration time was 30 ms.

PA spectra were acquired by scanning the excitation laser wavelength while recording the lock-in signal. Ten spectra were acquired and averaged. Data acquisition and processing were carried out using home-written Python software. More information about the photothermal technique can be found in Reference 45.

Ensemble PL and ASPL spectroscopy. Ensemble PL and ASPL spectra were acquired using the same microscope employed for photothermal absorption measurements. The output of the supercontinuum was focused onto specimens and induced PL or ASPL was collected with a 0.45 NA (Nikon) long working distance objective. Both PL and ASPL were filtered using dielectric filters (Semrock) to remove any excitation light. Spectra were acquired using a spectrometer (Acton SpectraPro, SP-2300, 150 groove/mm, 800 nm blaze), coupled to an electron multiplying

CCD camera (Andor, Ixon Ultra). Detuned PL (ASPL) spectra were acquired by changing the excitation wavelength $\Delta E_{\rm S}$ (ΔE) above (below) the energy of the emitting state. Ten PL or ASPL spectra were acquired, integrated between 400-600 nm, and averaged. All data were acquired and processed using purpose-built Python software.

Acknowledgements

This work is dedicated to the memory of Mansoor Sheik-Bahae. We thank the MURI:MARBLe project under the auspices of the Air Force Office of Scientific Research (Award No. FA9550-16-1-0362) for financial support. This work was also supported, in part, by the National Science Foundation under award DMR-1952841. MB acknowledges support from the Max Planck-UBC-UTokyo Center for Quantum Materials and Canada First Research Excellence Fund (CFREF) Quantum Materials and Future Technologies Program of the Stewart Blusson Quantum Matter Institute and the Natural Sciences and Engineering Research Council of Canada.

Author Contributions

Z. Z. and S. G. contributed equally to this work.

Notes

The authors declare no competing financial interest.

ASSOCIATED CONTENT

Supporting Information.

The Supporting Information is available free of charge at https://pubs.acs.org/

Literature-reported CsPbBr₃ phonon energies and associated electron-phonon coupling energies, representative STEM images of obtained CsPbBr₃ NCs, CsPbBr₃ NC ensemble linear absorption, PL spectra, and power-dependent ASPL at different wavelengths, schematic of instrumentation used to conduct PL, ASPL, and PA spectroscopies, PA and PL spectra of CsPbBr₃ ensemble at different temperatures, table summarizing *T*-dependent absorption and peak PL energies along with corresponding full width at half maxima (FWHM) and Stokes shifts, CsPbBr₃ NC *T*-dependent PL FWHM and Stokes shifts, mathematical model for estimating η_{ASPL} based on PA, PL, and ASPL intensities, details of extractions of η_{ASPL} at different temperatures and different detuning energies, summary of ΔE -dependent η_{ASPL} at T=80 K and T=250 K, summary of T-dependent η_{ASPL} for ΔE_{S} =32 meV and ΔE_{S} =55 meV, details of QY measurements, details of femtosecond transient absorption up-conversion spectra of CsPbBr₃ NCs, PL and ASPL spectra from a CsPbBr₃ NC suspension.

REFERENCES

¹ Seletskiy, D. V.; Epstein, R.; Sheik-Bahae, M. Laser Cooling in Solids: Advances and Prospects. *Rep. Prog. Phys.* **2016**, *79* (9), 096401.

² Hehlen, M. P.; Meng, J.; Albrecht, A. R.; Lee, E. R.; Aram Gragossian; Love, S. P.; Hamilton, C. E.; Epstein, R. I.; Mansoor Sheik-Bahae. First Demonstration of an All-Solid-State Optical Cryocooler. *Light Sci. Appl.* **2018**, *7* (1), 15.

³ Kock, J.; Albrecht, A. R.; Epstein, R. I.; Mansoor Sheik-Bahae. Optical Refrigeration of Payloads to T < 125 K. *Opt. Lett.* **2022**, *47* (18), 4720-4720.

⁴Bowman, S. R. Lasers without Internal Heat Generation. *IEEE J. Quantum Electron.* **1999**, *35* (1), 115-122.

- ⁵ Nemova, G. Radiation-Balanced Lasers: History, Status, Potential. *Appl. Sci.* **2021**, *11* (16), 7539.
- ⁶ Pringsheim, P. Zwei Bemerkungen über Den Unterschied von Lumineszenz- Und Temperaturstrahlung. *Zeitschrift für Phys.* **1929**, *57* (11-12), 739-746.
- ⁷ Epstein, R. I.; Buchwald, M. I.; Edwards, B. C.; Gosnell, T. R.; Mungan, C. E. Observation of Laser-Induced Fluorescent Cooling of a Solid. *Nature* **1995**, *377* (6549), 500-503.
- ⁸ Melgaard, S. D.; Albrecht, A. R.; Hehlen, M. P.; Mansoor Sheik-Bahae. Solid-State Optical Refrigeration to Sub-100 Kelvin Regime. *Sci. Rep.* **2016**, *6* (1), 20380.
- ⁹ Sheik-Bahae, M.; Epstein, R. I. Can Laser Light Cool Semiconductors? *Phys. Rev. Lett.* **2004**, 92 (24), 247403.
- ¹⁰ Khurgin, J. B. Multi-Phonon-Assisted Absorption and Emission in Semiconductors and Its Potential for Laser Refrigeration. *Appl. Phys. Lett.* **2014**, *104* (22), 221115.
- ¹¹ Zhang, S.; Zhukovskyi, M.; Jankó, B.; Kuno, M. Progress in Laser Cooling Semiconductor Nanocrystals and Nanostructures. *NPG Asia Mater.* **2019**, *11* (1), 54.
- ¹² Mao, W.; Hall, C. R.; Bernardi, S.; Cheng, Y.-B.; Widmer-Cooper, A.; Smith, T. A.; Bach, U. Light-Induced Reversal of Ion Segregation in Mixed-Halide Perovskites. *Nature Mater.* 2020, 20 (1), 55-61.
- ¹³ Park, M.; Neukirch, A. J.; Reyes-Lillo, S. E.; Lai, M.; Ellis, S. R.; Dietze, D.; Neaton, J. B.; Yang, P.; Tretiak, S.; Mathies, R. A. Excited-State Vibrational Dynamics toward the Polaron in Methylammonium Lead Iodide Perovskite. *Nature Commun.* **2018**, *9* (1), 2525.

¹⁴ Guzelturk, B.; Winkler, T.; Van de Goor, T. W. J.; Smith, M. D.; Bourelle, S. A.; Feldmann, S.; Trigo, M.; Teitelbaum, S. W.; Steinrück, H.-G.; de la Pena, G. A.; Alonso-Mori, R.; Zhu, D.; Sato, T.; Karunadasa, H. I.; Toney, M. F.; Deschler, F.; Lindenberg, A. M. Visualization of Dynamic Polaronic Strain Fields in Hybrid Lead Halide Perovskites. *Nature Mater.* **2021**, *20* (5), 618-623.

¹⁵ Schilcher, M. J.; Robinson, P.; Abramovitch, D. J.; Tan, L. Z.; Rappe, A. M.; Reichman, D.
R.; Egger, D. The Significance of Polarons and Dynamic Disorder in Halide Perovskites. ACS
Energy Lett. 2021, 6 (6), 2162-2173.

¹⁶ Morozov, Y. V.; Zhang, S.; Brennan, M. C.; Boldizsár Jankó; Kuno, M. Photoluminescence Up-Conversion in CsPbBr₃ Nanocrystals. *ACS Energy Lett.* **2017**, *2* (10), 2514-2515.

¹⁷ Ye, Z.; Lin, X.; Wang, N.; Zhou, J.; Zhu, M.; Qin, H.; Peng, X. Phonon-Assisted Up-Conversion Photoluminescence of Quantum Dots. *Nature Commun.* **2021**, *12* (1), 4283.

¹⁸ Shibata, K.; Yan, J.; Hazama, Y.; Chen, S.; Akiyama, H. Exciton Localization and Enhancement of the Exciton-LO Phonon Interaction in a CsPbBr₃ Single Crystal. *J. Phys. Chem. C* **2020**, *124* (33), 18257-18263.

¹⁹ Ramade, J.; Andriambariarijaona, L. M.; Steinmetz, V.; Goubet, N.; Legrand, L.; Barisien, T.; Bernardot, F.; Testelin, C.; Lhuillier, E.; Bramati, A.; Chamarro, M. Exciton-Phonon Coupling in a CsPbBr₃ Single Nanocrystal. *Appl. Phys. Lett.* **2018**, *112* (7), 072104.

²⁰ Iaru, C. M.; Geuchies, J. J.; Koenraad, P. M.; Vanmaekelbergh, D.; Silov, A. Yu. Strong Carrier-Phonon Coupling in Lead Halide Perovskite Nanocrystals. *ACS Nano* **2017**, *11* (11), 11024-11030.

²¹ Saran, R.; Amelie Heuer-Jungemann; Kanaras, A. G.; Curry, R. J. Giant Bandgap Renormalization and Exciton-Phonon Scattering in Perovskite Nanocrystals. *Adv. Opt. Mater.* **2017**, *5* (17), 1700231.

- ²² Shinde, A.; Richa Gahlaut; Shailaja Mahamuni. Low-Temperature Photoluminescence Studies of CsPbBr₃ Quantum Dots. *J. Phys. Chem. C* **2017**, *121* (27), 14872-14878.
- ²³ Cho, K.; Tahara, H.; Yamada, T.; Hidekatsu Suzuura; Terumasa Tadano; Sato, R.; Masaki Saruyama; Hideki Hirori; Teranishi, T.; Kanemitsu, Y. Exciton-Phonon and Trion-Phonon Couplings Revealed by Photoluminescence Spectroscopy of Single CsPbBr₃ Perovskite Nanocrystals. *Nano Lett.* **2022**, *22* (18), 7674-7681.
- ²⁴ Rainò, G.; Yazdani, N.; Boehme, S. C.; Kober-Czerny, M.; Zhu, C.; Krieg, F.; Rossell, M. D.; Erni, R.; Wood, V.; Infante, I.; Kovalenko, M. V. Ultra-Narrow Room-Temperature Emission from Single CsPbBr₃ Perovskite Quantum Dots. *Nature Commun.* **2022**, *13* (1), 2587.
- ²⁵ Peter Theodore Landsberg. *Recombination in Semiconductors*; Cambridge University Press: Cambridge, 2003.
- ²⁶ Yu, P. Y.; Cardona, M. Fundamentals of Semiconductors; Springer, 2010.
- ²⁷ Hopper, T. R.; Gorodetsky, A.; Frost, J. M.; Müller, C.; Lovrincic, R.; Bakulin, A. A. Ultrafast Intraband Spectroscopy of Hot-Carrier Cooling in Lead-Halide Perovskites. *ACS Energy Lett.* **2018**, *3* (9), 2199-2205.
- ²⁸ Fu, J.; Xu, Q.; Han, G.; Wu, B.; Huan, C. H. A.; Leek, M. L.; Sum, T. C. Hot Carrier Cooling Mechanisms in Halide Perovskites. *Nature Commun.* **2017**, *8* (1), 1300.

²⁹ Li, M.; Bhaumik, S.; Goh, T. W.; Kumar, M. S.; Yantara, N.; Grätzel, M.; Mhaisalkar, S.; Mathews, N.; Sum, T. C. Slow Cooling and Highly Efficient Extraction of Hot Carriers in Colloidal Perovskite Nanocrystals. *Nature Commun.* **2017**, *8* (1), 14350.

³⁰ Yang, Y.; Ostrowski, D. P.; France, R. M.; Zhu, K.; van de Lagemaat, J.; Luther, J. M.; Beard, M. C. Observation of a Hot-Phonon Bottleneck in Lead-Iodide Perovskites. *Nature Photonics* **2015**, *10* (1), 53-59.

³¹ Frost, J. M.; Whalley, L. D.; Walsh, A. Slow Cooling of Hot Polarons in Halide Perovskite Solar Cells. *ACS Energy Lett.* **2017**, *2* (12), 2647-2652.

³² Jadczak, J.; Bryja, L.; Kutrowska-Girzycka, J.; Kapuściński, P.; Bieniek, M.; Huang, Y. S.; Hawrylak, P. Room Temperature Multi-Phonon Upconversion Photoluminescence in Monolayer Semiconductor WS₂. *Nature Commun.* **2019**, *10* (1), 107.

³³ Akizuki, N.; Aota, S.; Mouri, S.; Matsuda, K.; Miyauchi, Y. Efficient Near-Infrared Up-Conversion Photoluminescence in Carbon Nanotubes. *Nature Commun.* **2015**, *6* (1), 8920

³⁴ Gauck, H.; Gfroerer, T. H.; Renn, M. J.; Cornell, E. A.; Bertness, K. A. External Radiative Quantum Efficiency of 96% from a GaAs / GaInP Heterostructure. *Appl. Phys. A.* **1997**, *64* (2), 143-147.

³⁵ Bender, D. A.; Cederberg, J. G.; Wang, C.; Mansoor Sheik-Bahae. Development of High Quantum Efficiency GaAs/GaInP Double Heterostructures for Laser Cooling. *Appl. Phys. Lett.* 2013, 102 (25), 252102.

³⁶ Zhang, J.; Li, D.; Chen, R.; Xiong, Q. Laser Cooling of a Semiconductor by 40 Kelvin. *Nature* **2013**, 493 (7433), 504-508.

³⁷ Morozov, Y. V.; Zhang, S.; Pant, A.; Boldizsár Jankó; Melgaard, S. D.; Bender, D. A.; Pauzauskie, P. J.; Kuno, M. Can Lasers Really Refrigerate CdS Nanobelts? *Nature* 2019, 570 (7762), E60-E61.

- ³⁸ Ha, S.-T.; Shen, C.; Zhang, J.; Xiong, Q. Laser Cooling of Organic-Inorganic Lead Halide Perovskites. *Nature Photonics* **2015**, *10* (2), 115-121.
- ³⁹ Roman, B. J.; Noel Mireles Villegas; Lytle, K.; Sheldon, M. Optically Cooling Cesium Lead Tribromide Nanocrystals. *Nano Lett.* **2020**, *20* (12), 8874-8879.
- Imran, M.; Ijaz, P.; Goldoni, L.; Maggioni, D.; Petralanda, U.; Prato, M.; Almeida, G.; Infante,
 I.; Manna, L. Simultaneous Cationic and Anionic Ligand Exchange for Colloidally Stable
 CsPbBr₃ Nanocrystals. *ACS Energy Lett.* 2019, 4 (4), 819-824.
- ⁴¹ Ding, Y.; Zhang, Z.; Toso, S.; Gushchina, I.; Vadim Trepalin; Shi, K.; Peng, J. W.; Kuno, M. Mixed Ligand Passivation as the Origin of Near-Unity Emission Quantum Yields in CsPbBr₃ Nanocrystals. *J. Am. Chem. Soc.* **2023**, *145* (11), 6362-6370.
- ⁴² Brennan, M. C.; Herr, J. E.; Nguyen-Beck, T. S.; Zinna, J.; Draguta, S.; Rouvimov, S.; Parkhill, J.; Kuno, M. Origin of the Size-Dependent Stokes Shift in CsPbBr₃ Perovskite Nanocrystals. *J. Am. Chem. Soc.* **2017**, *139* (35), 12201-12208.
- ⁴³ Brennan, M. C.; Forde, A.; Zhukovskyi, M.; Baublis, A. J.; Morozov, Y. V.; Zhang, S.; Zhang, Z.; Kilin, D. S.; Kuno, M. Universal Size-Dependent Stokes Shifts in Lead Halide Perovskite Nanocrystals. *J. Phys. Chem. Lett.* **2020**, *11* (13), 4937-4944.
- ⁴⁴ Roman, B. J.; Sheldon, M. The Role of Mid-Gap States in All-Inorganic CsPbBr₃ Nanoparticle One Photon Up-Conversion. *Chem. Commun.* **2018**, *54* (50), 6851–6854.

⁴⁵ Adhikari, S.; Spaeth, P.; Kar, A.; Baaske, M. D.; Saumyakanti Khatua; Orrit, M. Photothermal Microscopy: Imaging the Optical Absorption of Single Nanoparticles and Single Molecules. *ACS Nano* **2020**, *14* (12), 16414-16445.

⁴⁶ Giblin, J.; Muhammad Ali Syed; Banning, M. T.; Kuno, M.; Hartland, G. V. Experimental Determination of Single CdSe Nanowire Absorption Cross Sections through Photothermal Imaging. *ACS Nano* **2010**, *4* (1), 358-364.

⁴⁷ Brennan, M. C.; Zinna, J.; Kuno, M. Existence of a Size-Dependent Stokes Shift in CsPbBr₃ Perovskite Nanocrystals. *ACS Energy Lett.* **2017**, *2* (7), 1487-1488.

⁴⁸ Draguta, S.; Thakur, S.; Morozov, Y. V.; Wang, Y.; Manser, J. S.; Kamat, P. V.; Kuno, M. Spatially Non-Uniform Trap State Densities in Solution-Processed Hybrid Perovskite Thin Films. *J. Phys. Chem. Lett.* **2016**, *7* (4), 715–721.

⁴⁹ Wang, C.; Li, C.-Y.; Hasselbeck, M. P.; Imangholi, B.; Sheik-Bahae, M. Precision, All-Optical Measurement of External Quantum Efficiency in Semiconductors. *J. Appl. Phys.* **2011**, *109* (9), 093108.

⁵⁰ Morozov, Y. V.; Draguta, S.; Zhang, S.; Cadranel, A.; Wang, Y.; Janko, B.; Kuno, M. Defect-Mediated CdS Nanobelt Photoluminescence Up-Conversion. *J. Phys. Chem. C* **2017**, *121* (30), 16607-16616.

⁵¹ Ament, L. J. P.; van Veenendaal, M.; Devereaux, T. P.; Hill, J. P.; van den Brink, J. Resonant Inelastic X-Ray Scattering Studies of Elementary Excitations. *Rev. Mod. Phys.* **2011**, *83* (2), 705-767.

⁵² Becker, M. A.; Vaxenburg, R.; Nedelcu, G.; Sercel, P. C.; Shabaev, A.; Mehl, M. J.; Michopoulos, J. G.; Lambrakos, S. G.; Bernstein, N.; Lyons, J. L.; Stöferle, T.; Mahrt, R. F.;

Kovalenko, M. V.; Norris, D. J.; Raino, G.; Efros, A. L. Bright triplet excitons in caesium lead halide perovskites. *Nature* **2018**, 553 (7687), 189-193.

⁵³ Sercel, P. C.; Lyons J. L.; Wickramaratne, D.; Vaxenburg, R.; Bernstein, N.; Efros, A. L. *Nano Letters* **2019** *19* (6), 4068-4077.